Proceedings Paper:
Xin, S, You, Y, Zhou, C orcid.org/0000-0002-6677-0855 et al. (2 more authors) (2017) A torque-controlled humanoid robot riding on a two-wheeled mobile platform. In: 2017 IEEE/RSJ International Conference on Intelligent Robots and Systems (IROS). 2017 IEEE/RSJ (IROS), 24-28 Sep 2017, Vancouver, BC, Canada. IEEE , pp. 1435-1442. ISBN 978-1-5386-2682-5

https://doi.org/10.1109/IROS.2017.8205945

A Torque-controlled Humanoid Robot Riding on a Two-wheeled Mobile Platform

Songyan Xin, Yangwei You, Chengxu Zhou, Cheng Fang, Nikos Tsagarakis

***Abstract*— This paper is motivated by the questions: What would happen if a humanoid robot is put on a Segway? Is it possible for the humanoid robot to use this transportation device that is specifically designed for human? Simulation involving a two-wheeled mobile platform (TWMP) and our humanoid robot COMAN (COmpliant HuMANoid Platform) shows that it is indeed feasible without any hardware modification. Regarding the implementation, the full dynamics of the humanoid robot is considered and quadratic optimization is employed to generate whole-body joint torques to realise two types of tasks according to the interaction type between the TWMP and the humanoid robot. The TWMP is considered as unknown disturbance and the humanoid robot has to keep balancing on it in the first type of task. On the contrary, the active movement of the humanoid robot is utilised as an interface to intuitively drive the TWMP in the second type of task. For both tasks, tracking the position of center of mass (CoM) and regulating the angular momentum around it are considered as primary objectives, stabilizing the posture of certain part of its body is optional. In addition, both tasks are repeated on uneven terrain to demonstrate the robustness of the control method.**

Fig. 1. COMAN riding on a two-wheeled mobile platform

I. Introduction

Humans are able to perform a wide variety of tasks and humanoid robots are created with the expectation to have comparable capability and versatility [1]. Most daily objects and tools are designed to fit in human size and in such a way can be easily handled and operated. Resembling the human body, humanoid robots can potentially take advantages of it, thereby avoiding the need to alter the environment or modify its own structure. Even though how to use human-oriented tools has been extensively studied in the manipulation tasks performed by robotic arms, few attentions have been drawn to those tools which are supposed to be operated by the lower limb or whole body of human. Wheeled mobile transportation platform is a very important tool of this kind. In general, wheeled platforms consume less energy and move faster than legged robots in terms of mobility, therefore it is necessary to investigate the manoeuvrability of them for humanoid robots.

Comparing to other wheeled mobile platforms, two-wheeled mobile platform (TWMP), well known as Segway™, is more convenient and lightweight. It has the advantages of small footprint, zero turning radius and relatively large carrying payload [2]. The modeling and control of TWMP have also been widely studied. In 2002, the Swiss Federal Institute of Technology built a scaled down prototype of a two-wheeled vehicle, named JOE, which is able to balance itself while tracking commanded velocity inputs [3]. At the same year, Segway™ Personal Transporter was brought to market as a new mobile platform for human transporting [2]. Different control methods were proposed to improve its performance [4]–[6].

To make use of the mobility of the wheeled platform for the humanoid robot, several attempts have been made. The Johnson Space Center developed a mobile manipulation system in which the upper body of the NASA/DARPA Robonaut system is attached to Segway™ robotic mobility platform yielding a dexterous, maneuverable humanoid [7], [8]. Recently, Boston Dynamics™ released a new robot, Handle, which is a wheel-leg hybrid robotic system that can take advantage of both humanoid robots and wheeled mobile robots. The Handle robot is an integrated system and the control algorithms has to treat it as a whole. In this paper, instead of modifying the humanoid robot, we are going to explore how to use the existing humanoid robot to operate the TWMP without additional hardware customization. More specifically, we attempt to make our humanoid robot COMAN (COmpliant HuMANoid Platform) operate the two-wheeled mobile platform as shown in Fig. 1. Hyungjik et al. have implemented similar idea on their position-controlled humanoid robot [9]. The humanoid robot can lean forward or backward to regulate its center of gravity to control the movement of mobile platform. But since the employed humanoid robot is position-controlled, it is difficult for the humanoid robot to resist large disturbance and perform compliant motions.

COMAN is actuated by passive compliance actuators

based on the series elastic actuation principle (SEA) [10]. Active compliance control has been applied to stabilize the humanoid robot for various tasks [11]. Besides that, it is also capable of operating in torque control mode. The whole-body dynamic model of the humanoid robot allows us to calculate required torques for a specific motion considering dynamic coupling effects. The passive compliance actuators can reject small perturbation and make the robot behaves compliantly.

Torque-controlled robots become more and more available and many related algorithms are developed. Passivity-based approaches [12], [13] compute admissible contact force and control commands under quasi-static assumptions without the need of full dynamic model. However, more dynamic motions can be handled by considering the full dynamic model of the robot [14]–[17]. What is common between these approaches is that they all regulate the position of the center of mass (CoM) of the robot to ensure that the robot does not fall while maintaining the contact forces in physically achievable range. To achieve better performance for balancing the robot, momentum-based controller was proposed [15], [18], [19]. In such approach, both CoM motion (i.e. linear momentum) and its angular momentum are controlled. Optimization methods [20]–[24] are used as a tool to calculate joint torques based on whole-body dynamics. Experiments on various robots shows impressive, human-like balancing behaviors [14], [25]–[28].

Based on the investigations in both research fields, we decided to use the whole-body dynamic torque control strategy to stabilize the humanoid robot on a TWMP and drive it. This paper is organized as follows. In Section II, the linearized model of TWMP was given and control method is proposed. Afterwards, the whole-body torque control framework of the humanoid robot is introduced in Section III. In Section IV, several tasks are demonstrated in Gazebo simulator (ODE-based rigid body simulator), and results are analysed. The paper ends with conclusions and an outlook of future works.

II. Model and Control Strategy of TWMP

The TWMP is actually a mobile inverted pendulum and its model have been widely studied in the field of autonomous robotics [3], [29], [30].

The mobile platform has three degrees of freedom (DoF): 1) the rotation about the the wheel axis, this movement is intrinsically unstable, the body part of the inverted pendulum tends to fall if given no control, 2) the linear movement in the heading direction, 3) the steering rotation which changes the heading of the robot.

The coordinate frame is shown in Fig. 2. Three coordinate frames are plotted in the figure: one world frame $\{F_w = \{x_w, y_w, z_w\}$, one intermediate frame $\{F'\} = \{x', y', z'\}$ and a local frame $\{F\} = \{x, y, z\}$. The dynamic of the robot can be fully described with six parameters: θ_P and ω_P stands for the pitch angle and angular velocity around the y axis. The mobile platform position and velocity in the heading direction is defined as x_M and v_M. Additionally, θ_Y and $\dot{\theta}_Y$ are the yaw angle and associated angular velocity around

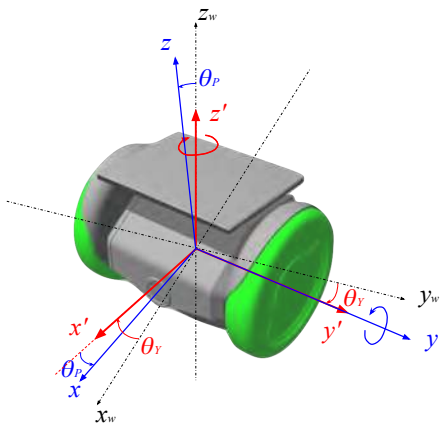

Fig. 2. The mobile inverted pendulum model

the z_w axis. The nonlinear dynamic model of the inverted pendulum model follows the equations given in [3], [5].

Linearizing the nonlinear model around the operating point($x_M = 0$, $v_M = 0$, $\theta_P = 0$, $\theta_Y = 0$) the system can be written in state-space form:

$$\dot{\boldsymbol{X}} = \boldsymbol{A}\boldsymbol{X} + \boldsymbol{B}\boldsymbol{u} \tag{1}$$

where $\boldsymbol{X} = [x_M, v_M, \theta_P, \omega_P, \theta_Y, \dot{\theta}_Y]^T$ denotes the state vector, $\boldsymbol{u} = [C_L, C_R]^T$ are input torques on left and right wheel.

The decoupling transformation developed in [3] decomposes the above system into two independent subsystems.

$$\begin{bmatrix} C_L \\ C_R \end{bmatrix} = \begin{bmatrix} 0.5 & 0.5 \\ 0.5 & -0.5 \end{bmatrix} \begin{bmatrix} C_P \\ C_Y \end{bmatrix} \tag{2}$$

One subsystem relates to the rotation and linear translation in sagittal plane:

$$\begin{bmatrix} \dot{x}_M \\ \dot{v}_M \\ \dot{\theta}_P \\ \dot{\omega}_P \end{bmatrix} = \boldsymbol{A}_P \begin{bmatrix} x_M \\ v_M \\ \theta_P \\ \omega_P \end{bmatrix} + \boldsymbol{B}_P C_P \tag{3}$$

The other subsystem describes the steering of the mobile robot in transverse plane:

$$\begin{bmatrix} \dot{\theta}_Y \\ \ddot{\theta}_Y \end{bmatrix} = \boldsymbol{A}_Y \begin{bmatrix} \theta_Y \\ \dot{\theta}_Y \end{bmatrix} + \boldsymbol{B}_Y C_Y \tag{4}$$

Then two independent controllers can be designed for each subsystem. For the sagittal plane inverted pendulum subsystem, the control goal is to achieve self-balancing without falling down. The yaw control goal is simply to regulate the turning rate to a desired value.

The design of the state-space feedback controllers follows textbook approaches which formulate a stable close-loop controller to drive the system state to the desired values.

The TWMP provides the user a command interface through which the user is able to send desired forward speeds and steering rates to control the platform directly.

III. WHOLE-BODY TORQUE CONTROLLER OF COMAN

The whole-body torque controller of humanoid robot is based on whole-body dynamics and formulated as a quadratic optimization problem to generate joint torques according to given tasks with respect to constraints, such as dynamic feasibility, friction cone, torque limits. Different weights are used to balance multiple tasks in the cost function without considering strict priorities among them. It is numerically robust and simple to implement. Hard constraints such as joint torque limits and friction cone limits are formulated as inequality constraints. We will give details about the controller starting from the Equation of Motion (EoM) of the humanoid robot:

$$\boldsymbol{M}(\boldsymbol{q})\ddot{\boldsymbol{q}} + \boldsymbol{h}(\boldsymbol{q}, \dot{\boldsymbol{q}}) = \boldsymbol{S}^T\boldsymbol{\tau} + \boldsymbol{J}_{\mathrm{c}}^T(\boldsymbol{q})\boldsymbol{\lambda} \tag{5}$$

with the inertia matrix $\boldsymbol{M}(\boldsymbol{q})$, the force vector $\boldsymbol{h}(\boldsymbol{q})$ which is sum of Coriolis, centrifugal and gravitational forces and the ground reaction force $\boldsymbol{\lambda}$, $\boldsymbol{J}_{\mathrm{c}}$ is corresponding Jacobian, $\boldsymbol{\tau}$ is joint torque, $\boldsymbol{q} = [\boldsymbol{q}_f^T, \boldsymbol{q}_r^T]^T$ represents the n DoF generalized coordinates which include the floating-base coordinates and body joint coordinates, and $\boldsymbol{S} = [\boldsymbol{0}_{n_r \times n_f}, \boldsymbol{I}_{n_r}]$ is a selection matrix which separates the $n_r = n - n_f$ actuated joints from the $n_f = 6$ floating-base DoF.

EoM (5) relates generalized acceleration $\ddot{\boldsymbol{q}}$, contact forces $\boldsymbol{\lambda}$ and joint torques $\boldsymbol{\tau}$ together. We choose $\boldsymbol{X} = [\ddot{\boldsymbol{q}}^T, \boldsymbol{\lambda}^T]^T$ as optimization variables for the following QP problem :

$$\min_{\boldsymbol{X}} \sum_{i=1}^{n} \omega_i ||\boldsymbol{A}_{\mathrm{i}}\boldsymbol{X} - \boldsymbol{b}_{\mathrm{i}}||^2 \tag{6}$$

subject to

$$\boldsymbol{M}_{\mathrm{f}}(\boldsymbol{q})\ddot{\boldsymbol{q}} + \boldsymbol{h}_{\mathrm{f}}(\boldsymbol{q}, \dot{\boldsymbol{q}}) = \boldsymbol{J}_{cf}^T(\boldsymbol{q})\boldsymbol{\lambda} \tag{7}$$

$$\boldsymbol{\tau} = \boldsymbol{S}(\boldsymbol{M}(\boldsymbol{q})\ddot{\boldsymbol{q}} + \boldsymbol{h}(\boldsymbol{q}, \dot{\boldsymbol{q}}) - \boldsymbol{J}_c^T(\boldsymbol{q})\boldsymbol{\lambda}) \in [\boldsymbol{\tau}_{\min}, \boldsymbol{\tau}_{\max}] \tag{8}$$

$$\boldsymbol{J}_c\ddot{\boldsymbol{q}} + \dot{\boldsymbol{J}}_c\dot{\boldsymbol{q}} = 0 \tag{9}$$

$$|\frac{f_x}{f_z}| \leq \mu,\ |\frac{f_y}{f_z}| \leq \mu \tag{10}$$

$$f_z > 0 \tag{11}$$

$$d_x^- \leq \frac{m_y}{f_z} \leq d_x^+,\ d_y^- \leq -\frac{m_x}{f_z} \leq d_y^+ \tag{12}$$

The objective function tries to minimize the sum of tracking error of tasks, but their relative importance is decided by corresponding weight ω_i. Tasks usually involve: motion tasks (regulating CoM position or tracking end-effectors' space trajectory), contact force tasks (optimizing contact force distribution) and joint torque tasks (assigning joint torques).

The constraints (7) and (8) ensure the dynamics feasibility and joint torque limits, the subscript f in (7) stands for the six DoF of floating base. (9) makes sure there is no slip in contact points. The contact wrench can be expressed as: $\boldsymbol{\lambda} = [f_x, f_y, f_z, m_x, m_y, m_z]^T$. The nonlinear friction cone is approximated as a linear polyhedral cone (10) which limits the contact force in feasible range with respect to the friction coefficient. (11) is the unilateral constraints which make sure the robot stay in contact with the ground. (12) restricts the ZMP inside support polygon which is defined within the limits $[d_x^-, d_x^+]$ and $[d_y^-, d_y^+]$.

To make the robot ride a self-balancing car, the task defined here is a motion task, regulating the linear and angular momentum and stabilize the torso posture. Considering the centroidal dynamics [31], the system's linear momentum $\boldsymbol{P}$ and angular momentum $\boldsymbol{L}$ is linear with the generalized velocity $\dot{\boldsymbol{q}}$:

$$\begin{bmatrix}\boldsymbol{P}\\ \boldsymbol{L}\end{bmatrix} = \boldsymbol{H}(\boldsymbol{q})\dot{\boldsymbol{q}} \tag{13}$$

with $\boldsymbol{H}$ is called the centroidal momentum matrix. Taking derivative of this equation will give:

$$\begin{bmatrix}\dot{\boldsymbol{P}}\\ \dot{\boldsymbol{L}}\end{bmatrix} = \boldsymbol{H}\ddot{\boldsymbol{q}} + \dot{\boldsymbol{H}}\dot{\boldsymbol{q}} \tag{14}$$

It is obvious that the changing rate of momentum $\dot{\boldsymbol{P}}$ and $\dot{\boldsymbol{L}}$ is linear function of $\ddot{\boldsymbol{q}}$. As a result, the objective function to track desired changing rate of momentum can be written as below:

$$\boldsymbol{A}_H = [\boldsymbol{H},\ \boldsymbol{0}],\ \boldsymbol{b}_H = \begin{bmatrix}\dot{\boldsymbol{P}}_{\mathrm{ref}}\\ \dot{\boldsymbol{L}}_{\mathrm{ref}}\end{bmatrix} - \dot{\boldsymbol{H}}\dot{\boldsymbol{q}} \tag{15}$$

Typically, reference changing rate of momentum could be defined as:

$$\begin{bmatrix}\dot{\boldsymbol{P}}_{\mathrm{ref}}\\ \dot{\boldsymbol{L}}_{\mathrm{ref}}\end{bmatrix} = \begin{bmatrix}\dot{\boldsymbol{P}}_{\mathrm{des}}\\ \dot{\boldsymbol{L}}_{\mathrm{des}}\end{bmatrix} + \boldsymbol{K}_{\mathrm{p}}^c \begin{bmatrix}\boldsymbol{C}_{\mathrm{des}} - \boldsymbol{C}\\ \boldsymbol{0}\end{bmatrix} + \boldsymbol{K}_{\mathrm{d}}^c \begin{bmatrix}\boldsymbol{P}_{\mathrm{des}} - \boldsymbol{P}\\ \boldsymbol{L}_{\mathrm{des}} - \boldsymbol{L}\end{bmatrix} \tag{16}$$

with $\boldsymbol{K}_p^c$ and $\boldsymbol{K}_d^c$ the gains of the PD feedback controller, $\boldsymbol{P}_{\mathrm{des}}$, $\boldsymbol{L}_{\mathrm{des}}$ the desired linear and angular momentum, and $\boldsymbol{C}$, $\boldsymbol{C}_{\mathrm{des}}$ the measured and desired CoM position.

The stabilization of torso posture in Cartesian space is formulated as:

$$\boldsymbol{A}_{\mathrm{cartesian}} = [\boldsymbol{J},\ \boldsymbol{0}],\ \boldsymbol{b}_{\mathrm{cartesian}} = \ddot{\boldsymbol{x}}_{\mathrm{ref}} - \dot{\boldsymbol{J}}\dot{\boldsymbol{q}} \tag{17}$$

with $\boldsymbol{J}$ the spacial Jacobian matrix corresponding to the frame attached to the torso. $\ddot{\boldsymbol{x}}_{\mathrm{ref}}$ is the reference angular acceleration which can be calculated by

$$\ddot{\boldsymbol{x}}_{\mathrm{ref}} = \ddot{\boldsymbol{x}}_{\mathrm{des}} + \boldsymbol{K}_{\mathrm{p}}^t \log_{SO(3)}(\boldsymbol{R}) + \boldsymbol{K}_{\mathrm{d}}^t(\dot{\boldsymbol{x}}_{\mathrm{des}} - \dot{\boldsymbol{x}}) \tag{18}$$

where $\dot{\boldsymbol{x}}_{\mathrm{des}}$ and $\ddot{\boldsymbol{x}}_{\mathrm{des}}$ are the desired torso angular velocity and acceleration, $\dot{\boldsymbol{x}}$ is the measured angular velocity, and $\boldsymbol{R}$ is the rotation matrix from current torso orientation to the desired orientation. The logarithmic map $log_{SO(3)}$ follows the definition defined in [32].

IV. SIMULATION

Several tasks are conducted to verify previously proposed control scheme. The humanoid robot used here is COMAN and its full dynamic model is used in the simulation. COMAN body has 29 DoF in total: 6 DoF for each leg, 3 DoF waist and 7 DoF for each arm. In the simulation, each

joint is torque controlled and the joint level controller is a combination of feed-forward term and feedback term:

$$\boldsymbol{\tau} = \boldsymbol{\tau}_{\text{des}} + \boldsymbol{K}_p^{\tau}(\boldsymbol{q}_{\text{des}} - \boldsymbol{q}) + \boldsymbol{K}_d^{\tau}(\dot{\boldsymbol{q}}_{\text{des}} - \dot{\boldsymbol{q}}) + \boldsymbol{K}_i^{\tau} \int (\boldsymbol{q}_{\text{des}} - \boldsymbol{q}) \tag{19}$$

Where $\boldsymbol{\tau}_{\text{des}}$ is the desired joint torque computed from inverse dynamics as (8), $\boldsymbol{q}_{\text{des}}$ and $\dot{\boldsymbol{q}}_{\text{des}}$ are the desired joint position and velocity integrated from the desire joint acceleration which is the forepart of the optimization variable (6). $\boldsymbol{K}_p^{\tau}$, $\boldsymbol{K}_d^{\tau}$ and $\boldsymbol{K}_i^{\tau}$ are PID gains for the feedback term. In the simulation, we don't use the feedback part and merely set feedback gains to zero. But the feed-back part is important in real robotic system considering modelling error and sensor noises. In those cases, the feed-forward torque dominates the control command while feedback torque are mainly used to stabilize the joint. The control frequency is 500 Hz for the humanoid.

The TWMP used in the simulation is the open source RoboSavvy™ self-balancing robotic platform [33]. Since provided a velocity command interface, we can send a predefined velocity profile to the platform and make it as test platform which could be used to test the stability of the humanoid robot. The first task is to make the humanoid robot act as a camera stabiliser. The second task is to let the humanoid robot drive the mobile platform to a desired location. In this task, no velocity command will be sent to the mobile platform.

A. Task: Balancing and Camera Stabilizing

The primary problem for COMAN riding on the mobile platform is to guarantee the stability when standing on the platform. It would not be a difficult task since the platform can stably carry the rider with its own controller. Even with certain amount of external disturbance and payload variation, it could work as well. Therefore, we would like to assign additional tasks to COMAN. In this simulation, other than merely standing on the platform, COMAN was also expected to act as a stabilizer for the camera mounted in its head in order to capture steady images. Note that COMAN and the mobile platform are two separate systems without knowing the control details of each other. For COMAN, it will treat the movement of the platform as external disturbance and should be able to cope with it properly. For the mobile platform, it will treat the movement of COMAN as disturbance as well.

For balancing of the humanoid robot, whole-body dynamics should be utilized to regulate the linear and angular momentum of the whole system as shown in Section III. The desired linear and angular momentum $\boldsymbol{P}_{\text{des}}$, $\boldsymbol{L}_{\text{des}}$ and their changing rates $\dot{\boldsymbol{P}}_{\text{des}}$, $\dot{\boldsymbol{L}}_{\text{des}}$ were set zero. And the desired CoM position $\boldsymbol{C}_{des}$ in this task was given in this way:

$$\begin{aligned} \boldsymbol{C}_{\text{des}}^{x,y} &= \frac{1}{2}(\boldsymbol{P}_L^{x,y} + \boldsymbol{P}_R^{x,y}) \\ \boldsymbol{C}_{\text{des}}^{z} &= z_c. \end{aligned} \tag{20}$$

where $\boldsymbol{P}_L$ and $\boldsymbol{P}_R$ were the locations of the two feet in the world frame. z_c was given constant CoM height, and it should be within the kinematic limits of the robot. The superscripts indicate the corresponding components. The x and y components of the desired CoM position were equal to the geometrical center of two feet, and the z component was set to be constant with respect to the ground frame. The consideration behind this was: we would like to keep the ground projection of CoM as far as possible away form the boundary of the feet. In addition, to stabilize the internal camera, CoM should not oscillate too much in the vertical direction with respect to the ground frame. In real system, these global references would be given by the localization system. And the image captured from the camera could be used as feedback to decide the reference height.

The camera is installed in the head of COMAN, which is relatively fixed with respect to the torso. To stabilize the camera means to control the torso orientation, which is described as (18). The desired orientation given here is identical to the ground frame. And the corresponding angular velocities and accelerations are zero.

$$\boldsymbol{R}_{\text{des}} = \boldsymbol{I}_3 \tag{21}$$

where $\boldsymbol{I}_3$ is a three dimensional identity matrix.

Desired linear velocity $v = A\sin(2\pi ft + \phi)$ in heading direction and turning rate $\omega = 0$ were sent to the mobile platform individually. t is time, A is amplitude, f is the ordinary frequency and ϕ is the phase at $t = 0$. Following the sine wave linear velocity and zero turning rate, the mobile platform will move forward and backward in sagital plane and evoke disturbance to the standing of COMAN.

To evaluate the balancing ability of COMAN, other than checking the fluctuation of torso orientation, we would like also to have an intuitive feeling by just comparing the images collected separately from the two cameras mounted on COMAN and the mobile platform. As Figure 3 shows, the two cameras were close to each other and both shot towards the wall. The performance of COMAN stabilizing the camera was very impressive as seen in Figure 4. The thumbnails in the above row comes from the camera of the mobile platform which vibrated a lot. On the contrary, the ones from COMAN's camera shown below were much more stable. The time interval between these images was 1.5 seconds for both cameras.

The pitch angles of COMAN toros and the TWMP were shown in Figure 5. The varying range of pitch angle of COMAN torso was approximately 10 persent of the one measured from the TWMP, which was a large improvement.

B. Task: Riding the TWMP

One fantastic thing of the TWMP is that human riders can head to desired directions by leaning their bodies. To imitate this skill, COMAN was controlled to shift its CoM position forward and backward to regulate the forward velocity of the TWMP (see Figure 6). For turning, there are different kinds of devices for human rider to send the steering command, such as handlebar or twisting pedal. To be consistent with the way of regulating forward velocity, here we detect the force distribution on the left and right wheels caused by shifting

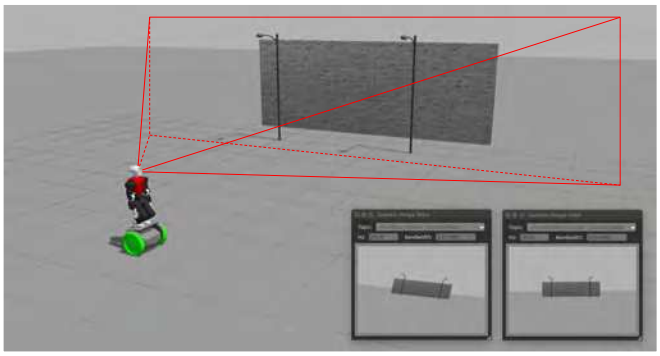

Fig. 3. The simulation setup. At the right bottom, views of the cameras are displayed: the left one is from the camera installed on the TWMP and the right one is from the one in the head of COMAN.

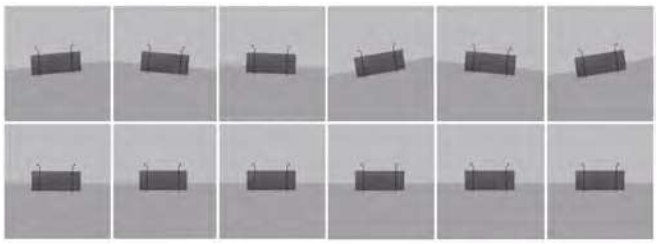

Fig. 4. Comparison between camera images (interval 1.5 seconds, the above row came from the camera mounted on the TWMP and below was form the one in the head of COMAN).

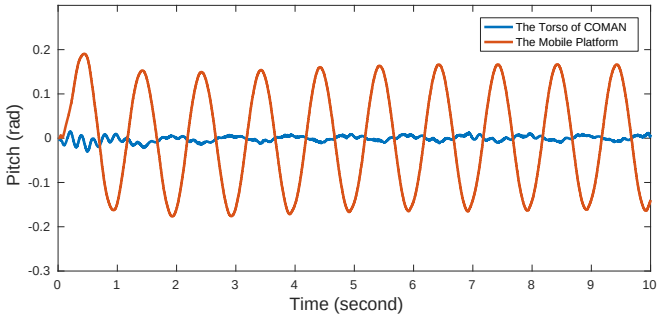

Fig. 5. Comparison between pitch angles of COMAN toros and the TWMP

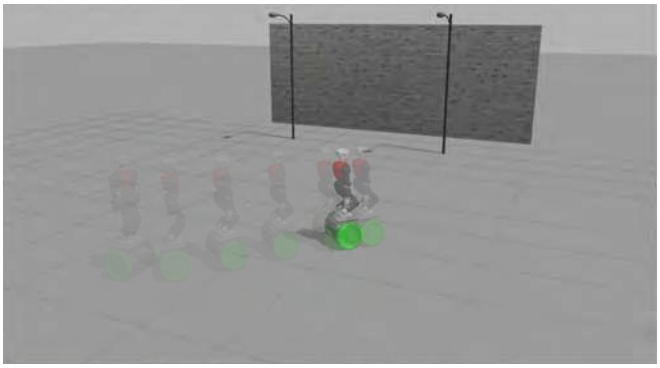

Fig. 6. COMAN drove the TWMP from the initial pose $[0, 0, 0]^T$ to the goal pose $[2, 2, \pi/4]^T$.

COMAN body left and right. According to the distribution, a steering command was generated by the TWMP and then it would turn to the direction that COMAN wished to go.

To testify the feasibility of the aforementioned control strategy, we commanded COMAN to drive the TWMP to a desired pose $\boldsymbol{P}_{des} = [x, y, \theta]^T$ which was given here as $\boldsymbol{P}_{des} = [2, 2, \pi/4]^T$ expressed in global frame. COMAN started from a initial pose $\boldsymbol{P}_{ini} = [0, 0, 0]^T$ and drove to the goal pose by shifting its CoM.

The tracking error used to generate CoM offset of COMAN was defined as $\boldsymbol{e} = [e_x, e_y, e_\theta]^T = \boldsymbol{P}_{\text{des}} - \boldsymbol{P}_{\text{cur}}$, and $\boldsymbol{P}_{\text{cur}}$ was the current pose of the TWMP. The control law was as below:

$$\begin{aligned} \Delta x &= K_x \sqrt{e_x^2 + e_y^2} \\ \Delta y &= K_y e_y + K_\theta e_\theta \end{aligned} \tag{22}$$

where Δx and Δy were CoM shifts from the center of the feet in the foot local frame. K_x, K_y and K_θ were feedback gains. Δx was in the forward direction which would affect the forward velocity while Δy was along lateral direction and related to the turning rate. To be noted, the calculated COM shifts would be truncated if they were out of the support polygon.

Apart from reaching to a goal pose, we also expected the torso of COMAN to be upright and head forward with respect to the TWMP all the way. Taking the turning of the TWMP into consideration, the desired orientation of COMAN was defined as:

$$\boldsymbol{R}_{\text{des}} = \boldsymbol{R}_z(\boldsymbol{P}_{\text{cur}}^{\theta}) \tag{23}$$

where $\boldsymbol{R}_z(\theta)$ was an elemental rotation matrix that rotates a vector by an angle θ about the z axis. $\boldsymbol{P}_{\text{cur}}^{\theta}$ is the current orientation of the TWMP.

The tracking data of the TWMP pose in this simulation is given in Fig. 7. COMAN successfully drove the TWMP to the goal location. And the corresponding CoM shift is shown in Figure 8. At the beginning, the commands were truncated because of the feet size limits. These limits prevent the humanoid robot shifting too much which would result the robot tilting on the TWMP.

C. Uneven Terrain

The previous simulations were performed on flat ground. In this part, we would like to challenge the proposed controller on uneven terrain.

1) Balancing and Camera Stabilizing: The setup of this simulation was similar with Section IV-A except that COMAN had to deal with additional disturbances introduced by the terrain (see Figure 9). Figure 10 shows that the image taken from the TWMP shook a lot and deviated from the target while the camera on COMAN still faced the right direction. The image deviation was because here the yaw regulation of the TWMP had no feedback control and would gradually drift away under the disturbance of uneven terrain. The pitch angles of COMAN torso and TWMP are shown in Figure 11. Much smaller fluctuation of COMAN torso was observed compared with the TWMP, similar with the result on flat ground.

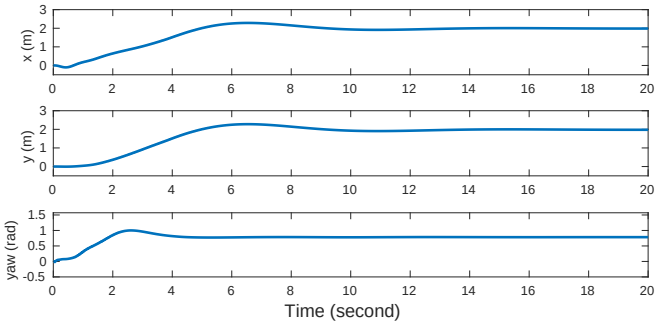

Fig. 7. The pose of the TWMP. It started from the initial pose $[0, 0, 0]^T$ and reached the final pose $[2, 2, \pi/4]^T$ after about 10 seconds.

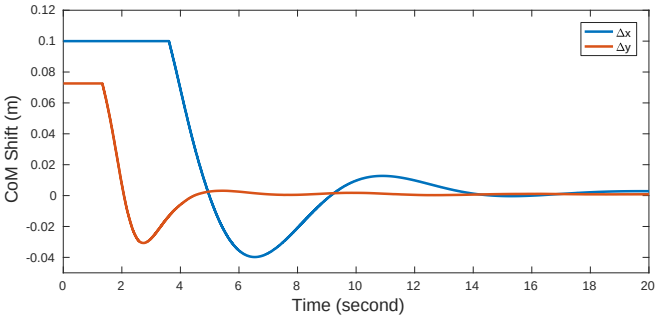

Fig. 8. The CoM shift of COMAN.

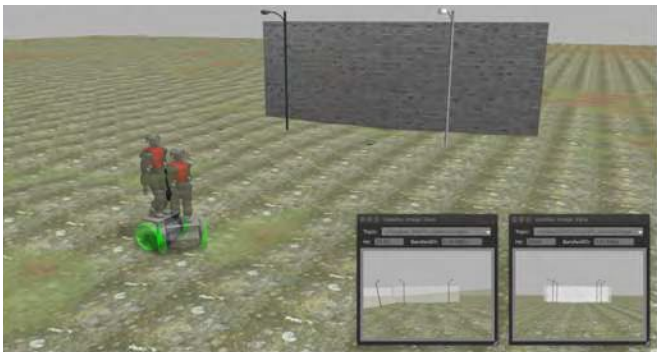

Fig. 9. Snapshot of the simulation on uneven terrain

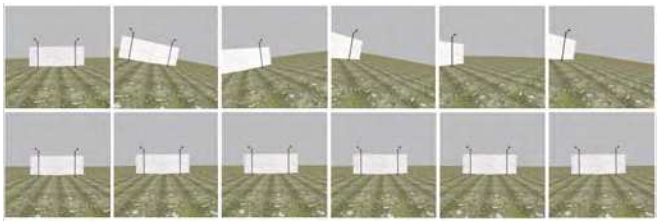

Fig. 10. Comparison between camera images. The above row comes from the camera mounted on the mobile platform and the below row is taken form the one in the head of COMAN (interval 3 seconds).

2) Riding the TWMP: The initial pose and goal pose set in this simulation were the same with Section IV-B (see Figure 12). The result in Figure 13 shows COMAN successfully reached the desired pose. And the corresponding CoM shift is shown in Figure 14. That the CoM shift did not converge to zero at the end is because COMAN needed to resist the inclination of the terrain at the goal location and keep the TWMP staying on the slope.

V. Conclusion and Future Work

A. Conclusion

In this paper we controlled the humanoid robot COMAN to perform two different tasks by utilising the transportation tool TWMP. The first one is to stabilize the camera which is installed in its head while balancing on the TWMP. Another task is to drive the TWMP to the desired location. Both tasks are performed on even terrain and uneven terrain.The humanoid robot successfully demonstrated its ability to utilise device designed for human and its versatility and adaptivity to different tasks and environment.

B. Future Works

With balancing and locomotion abilities demonstrated in this paper, as a natural extension, we would like to explore more tasks such as going down stairs, object manipulation, cooperation with human co-workers or other robots.

Another issue is the utilization of angular momentum. In these tasks, we simply set the desired angular momentum to zero, which helped to stabilize the body of COMAN. However, we found that it would hinder the operation of the TWMP. When TWMP tried to accelerate, it would tend to lean forward which would cause the changing of angular momentum of COMAN. As a result, COMAN would counteract the changing and slow down the acceleration of TWMP. It should be a better choice to define the desired angular momentum of COMAN according to the expected movement of the whole system.

In addition, as shown in the camera stabilizing simulation, this system is a perfect platform for capturing stable image information about the world around it and therefore should serve well for environment mapping and localization of itself.

Acknowledgment

This work is supported by the European Horizon 2020 robotics program CogIMon (ICT-23-2014 under grant agreement 644727).

References

[1] B. Siciliano and O. Khatib, *Springer handbook of robotics*. Springer Science & Business Media, 2008.

[2] H. G. Nguyen, J. Morrell, K. D. Mullens, A. B. Burmeister, S. Miles, N. Farrington, K. M. Thomas, and D. W. Gage, "Segway robotic mobility platform," in *Optics East*. International Society for Optics and Photonics, 2004, pp. 207–220.

[3] F. Grasser, A. D'arrigo, S. Colombi, and A. C. Rufer, "Joe: a mobile, inverted pendulum," *IEEE Transactions on industrial electronics*, vol. 49, no. 1, pp. 107–114, 2002.

[4] X. Ruan and J. Cai, "Fuzzy backstepping controllers for two-wheeled self-balancing robot," in *Informatics in Control, Automation and Robotics, 2009. CAR'09. International Asia Conference on*. IEEE, 2009, pp. 166–169.

[5] C.-C. Tsai, H.-C. Huang, and S.-C. Lin, "Adaptive neural network control of a self-balancing two-wheeled scooter," *IEEE Transactions on Industrial Electronics*, vol. 57, no. 4, pp. 1420–1428, 2010.

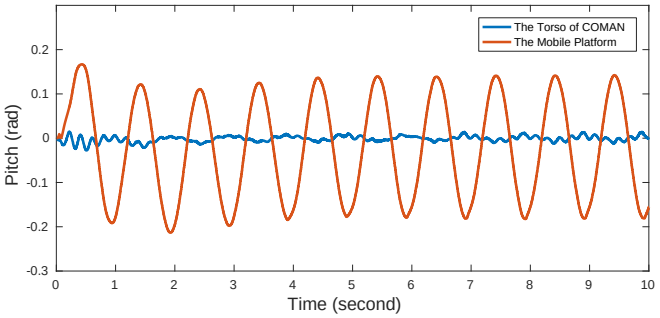

Fig. 11. Comparison between pitch angles of COMAN torso and the TWMP on uneven terrain

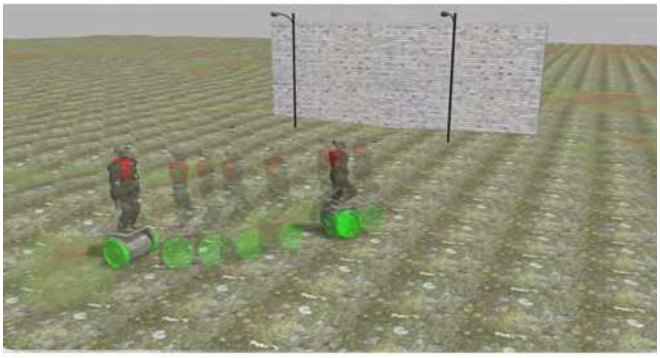

Fig. 12. COMAN drove the TWMP from the initial pose $[0, 0, 0]^T$ to the goal pose $[2, 2, \pi/4]^T$ on uneven terrain.

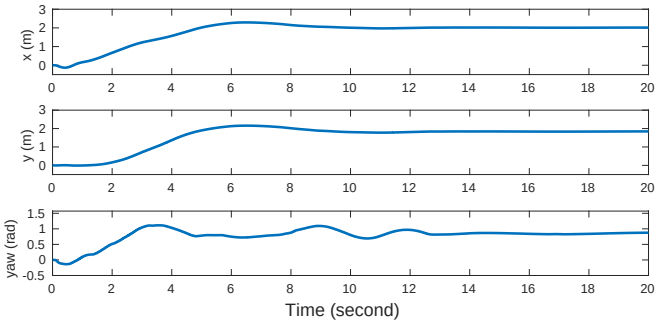

Fig. 13. The pose of the TWMP. It started from the initial pose $[0, 0, 0]^T$ and reached the final pose $[2, 2, \pi/4]^T$ after about 15 seconds.

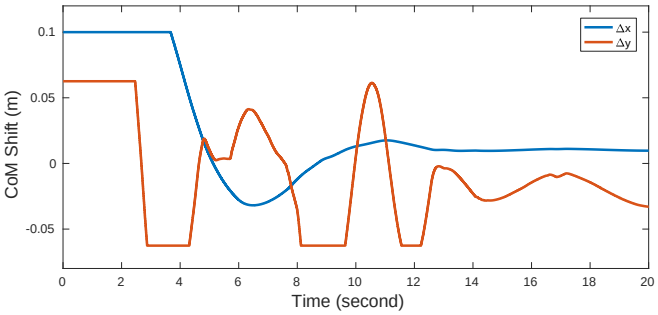

Fig. 14. The CoM shift of COMAN on uneven terrain

[6] J.-X. Xu, Z.-Q. Guo, and T. H. Lee, "Design and implementation of integral sliding-mode control on an underactuated two-wheeled mobile robot," *IEEE Transactions on industrial electronics*, vol. 61, no. 7, pp. 3671–3681, 2014.

[7] R. O. Ambrose, R. T. Savely, S. M. Goza, P. Strawser, M. A. Diftler, I. Spain, and N. Radford, "Mobile manipulation using nasa's robonaut," in *Robotics and Automation, 2004. Proceedings. ICRA'04. 2004 IEEE International Conference on*, vol. 2. IEEE, 2004, pp. 2104–2109.

[8] M. A. Diftler, R. O. Ambrose, K. S. Tyree, S. Goza, and E. Huber, "A mobile autonomous humanoid assistant," in *Humanoid Robots, 2004 4th IEEE/RAS International Conference on*, vol. 1. IEEE, 2004, pp. 133–148.

[9] H. Lee, H. J. Choi, J. H. Park, J. H. Lee, and S. Jung, "Center of gravity based control of a humanoid balancing robot for boxing games: Balbot v," in *ICCAS-SICE, 2009*. IEEE, 2009, pp. 124–128.

[10] N. G. Tsagarakis, S. Morfey, G. M. Cerda, L. Zhibin, and D. G. Caldwell, "Compliant humanoid coman: Optimal joint stiffness tuning for modal frequency control," in *Robotics and Automation (ICRA), 2013 IEEE International Conference on*. IEEE, 2013, pp. 673–678.

[11] C. Zhou, Z. Li, X. Wang, N. Tsagarakis, and D. Caldwell, "Stabilization of bipedal walking based on compliance control," *Autonomous Robots*, vol. 40, no. 6, pp. 1041–1057, 2016.

[12] S.-H. Hyon, J. G. Hale, and G. Cheng, "Full-body compliant human–humanoid interaction: balancing in the presence of unknown external forces," *IEEE Transactions on Robotics*, vol. 23, no. 5, pp. 884–898, 2007.

[13] C. Ott, M. A. Roa, and G. Hirzinger, "Posture and balance control for biped robots based on contact force optimization," in *Humanoid Robots (Humanoids), 2011 11th IEEE-RAS International Conference on*. IEEE, 2011, pp. 26–33.

[14] B. J. Stephens and C. G. Atkeson, "Dynamic balance force control for compliant humanoid robots," in *Intelligent Robots and Systems (IROS), 2010 IEEE/RSJ International Conference on*. IEEE, 2010, pp. 1248–1255.

[15] S.-H. Lee and A. Goswami, "A momentum-based balance controller for humanoid robots on non-level and non-stationary ground," *Autonomous Robots*, vol. 33, no. 4, pp. 399–414, 2012.

[16] L. Righetti, J. Buchli, M. Mistry, M. Kalakrishnan, and S. Schaal, "Optimal distribution of contact forces with inverse-dynamics control," *The International Journal of Robotics Research*, vol. 32, no. 3, pp. 280–298, 2013.

[17] C. G. A. Salman Faraji, Soha Pouya and A. J. Ijspeert, "Versatile and robust 3d walking with a simulated humanoid robot (atlas) a model predictive control approach," *IEEE International Conference on Robotics and Automation*, 2014.

[18] A. Macchietto, V. Zordan, and C. R. Shelton, "Momentum control for balance," *ACM Transactions on graphics (TOG)*, vol. 28, no. 3, p. 80, 2009.

[19] S.-H. Lee and A. Goswami, "Ground reaction force control at each foot: A momentum-based humanoid balance controller for non-level and non-stationary ground," in *Intelligent Robots and Systems (IROS), 2010 IEEE/RSJ International Conference on*. IEEE, 2010, pp. 3157–3162.

[20] M. de Lasa, I. Mordatch, and A. Hertzmann, "Feature-based locomotion controllers," in *ACM Transactions on Graphics (TOG)*, vol. 29, no. 4. ACM, 2010, p. 131.

[21] M. Hutter, M. A. Hoepflinger, C. Gehring, M. Bloesch, C. D. Remy, and R. Siegwart, "Hybrid operational space control for compliant legged systems," *Robotics*, p. 129, 2013.

[22] M. Hutter, H. Sommer, C. Gehring, M. Hoepflinger, M. Bloesch, and R. Siegwart, "Quadrupedal locomotion using hierarchical operational space control," *The International Journal of Robotics Research*, p. 0278364913519834, 2014.

[23] A. Escande, N. Mansard, and P.-B. Wieber, "Hierarchical quadratic programming: Fast online humanoid-robot motion generation," *The International Journal of Robotics Research*, vol. 33, no. 7, pp. 1006–1028, 2014.

[24] A. Herzog, N. Rotella, S. Mason, F. Grimminger, S. Schaal, and L. Righetti, "Momentum control with hierarchical inverse dynamics on a torque-controlled humanoid," *Autonomous Robots*, vol. 40, no. 3, pp. 473–491, 2016.

[25] A. Herzog, L. Righetti, F. Grimminger, P. Pastor, and S. Schaal, "Balancing experiments on a torque-controlled humanoid with hierarchical inverse dynamics," in *Intelligent Robots and Systems (IROS 2014),*

2014 IEEE/RSJ International Conference on. IEEE, 2014, pp. 981–988.

[26] S. Kuindersma, R. Deits, M. Fallon, A. Valenzuela, H. Dai, F. Permenter, T. Koolen, P. Marion, and R. Tedrake, "Optimization-based locomotion planning, estimation, and control design for the atlas humanoid robot," *Autonomous Robots*, vol. 40, no. 3, pp. 429–455, 2016.

[27] T. Koolen, S. Bertrand, G. Thomas, T. de Boer, T. Wu, J. Smith, J. Englsberger, and J. Pratt, "Design of a momentum-based control framework and application to the humanoid robot atlas," *International Journal of Humanoid Robotics*, vol. 13, no. 01, p. 1650007, 2016. [Online]. Available: http://www.worldscientific.com/doi/abs/10.1142/S0219843616500079

[28] B. Henze, A. Dietrich, and C. Ott, "An approach to combine balancing with hierarchical whole-body control for legged humanoid robots," *IEEE Robotics and Automation Letters*, vol. 1, no. 2, pp. 700–707, 2016.

[29] Y.-S. Ha *et al.*, "Trajectory tracking control for navigation of the inverse pendulum type self-contained mobile robot," *Robotics and autonomous systems*, vol. 17, no. 1-2, pp. 65–80, 1996.

[30] S.-C. Lin and C.-C. Tsai, "Development of a self-balancing human transportation vehicle for the teaching of feedback control," *IEEE Transactions on Education*, vol. 52, no. 1, pp. 157–168, 2009.

[31] D. E. Orin, A. Goswami, and S.-H. Lee, "Centroidal dynamics of a humanoid robot," *Autonomous Robots*, vol. 35, no. 2-3, pp. 161–176, 2013.

[32] F. Bullo and R. Murray, "Proportional derivative (pd) control on the euclidean group," in *European Control Conference*, vol. 2, 1995, pp. 1091–1097.

[33] R. Ltd. (2017) Robosavvy-balance. [Online]. Available: http://wiki.ros.org/Robots/RoboSavvy-Balance